

Tissue removal inside the beating heart using a robotically delivered metal MEMS tool

Nikolay V. Vasilyev¹, Andrew H. Gosline¹, Arun Veeramani², Ming Ting Wu², Gregory P. Schmitz², Richard T. Chen², Veaceslav Arabagi¹, Pedro J. del Nido¹ and Pierre E. Dupont¹

Abstract

A novel robotic tool is proposed to enable the surgical removal of tissue from inside the beating heart. The tool is manufactured using a unique metal MEMS process that provides the means to fabricate fully assembled devices that incorporate micron-scale features in a millimeter scale tool. The tool is integrated with a steerable curved concentric tube robot that can enter the heart percutaneously through peripheral vessels. Incorporating both irrigation and aspiration, the tissue removal system is capable of extracting substantial amounts of tissue under teleoperated control by first morseling it and then transporting the debris out of the heart through the lumen of the robot. Tool design and robotic integration are described, and ex vivo and in vivo large animal experimental results are presented.

Keywords

Robotic tool, MEMS process, heart surgery, tissue removal

1. Introduction

Surgical robotic systems are gaining popularity in clinical practice due to procedural benefits such as improved dexterity, motion scaling, tremor cancellation, and enhanced or augmented displays. Clinical benefits of these surgical robots are less invasive access to the surgical site and minimal trauma to neighboring structures, which result in less postoperative pain and faster recovery for a patient. In the specific case of cardiac procedures performed inside the heart, robotically-assisted minimally invasive surgery eliminates the need to cut open the chest (full sternotomy or thoracotomy) and requires only small stab incisions between the ribs, while also enabling the precise repair of intracardiac structures, such as valves (Modi et al., 2009). However, current robotically-assisted cardiac surgical procedures still require use of cardiopulmonary bypass (a heart-lung machine) in order to stop the heart and perform the repair inside its drained chambers. This may result in perioperative complications, especially in small children (Menache et al., 2002; Gander et al., 2010).

In parallel to the development of minimally invasive cardiac surgical procedures, catheter-based interventions have been evolving rapidly. Catheters can be introduced percutaneously (through a skin puncture) and advanced toward cardiac chambers via peripheral and then central vessels under X-ray fluoroscopy guidance. This eliminates the need

of any chest incision and often only requires local anesthesia at the site of puncture. While the introduction of catheters has transformed interventional cardiology practice by enabling device manipulation and deployment inside the beating heart under image guidance, many procedures remain possible only by open surgery on the stopped heart.

1.1. Engineering challenges

Despite recent advances in catheter technology, including the introduction of catheter-based robotic systems (Ikeuchi and Ikuta, 2009; Camarillo et al., 2008, 2009; Jayender et al., 2009; Kesner and Howe, 2011), catheters are not designed to apply significant amounts of force to the tissue, especially in the direction lateral to the main axis. In addition, stable positioning of the catheter tip on moving intracardiac targets can be challenging (Kesner and Howe, 2011).

Concentric tube robots are a relatively new class of continuum robots that consist of pre-curved elastic tubes in a

¹Cardiovascular Surgery, Boston Children's Hospital, Harvard Medical School, USA

²Microfabrica Inc., Van Nuys, CA, USA

Corresponding author:

Nikolay V. Vasilyev, Cardiovascular Surgery, Boston Children's Hospital, Harvard Medical School, Boston, MA, 02115, USA.
Email: Nikolay.Vasilyev@childrens.harvard.edu

telescoping arrangement (Rucker et al., 2010; Dupont et al., 2010). Active shape change is achieved by relative rotation and translation of the tubes at their base. Since they can be constructed with diameters similar to those of catheters and yet offer greater stiffness combined with the capability of shape control along their entire length, they provide an effective tool delivery technology for reconstructive procedures inside the beating heart (Gosline et al., 2012a, 2012b; Vasilyev et al., 2012, 2013).

Surgical reconstructive procedures are often comprised of a combination of two tasks: *tissue removal* in which specific portions of tissue are excised and removed from the body and *tissue approximation* in which two pieces of tissue are brought into contact and affixed to each other, e.g. by suture. While for some minimally invasive surgical applications, for example, bronchial endoscopy (Simaan et al., 2009) and laparoscopy (Madhani et al., 1998), it is possible to develop robotic tool delivery systems that use adapted endoscopic surgical tools to perform these tasks in a manner comparable to open surgery, the environment of the beating heart requires a different approach.

First, the procedure is performed in the bloodstream under ultrasound and X-ray fluoroscopy guidance making visualization and tool control difficult and requiring the use of imaging-compatible instrument materials (Huang et al., 2007). Secondly, tool manipulations cannot interfere with heart function, for example, by obstructing blood flow or by impairing electrical activity of the heart and inducing arrhythmias. Therefore, there is a clear need for appropriate tools for performing the surgical tasks of tissue removal and tissue approximation inside the beating heart.

1.2. Clinical significance

Prior work by our group presented the design of a robotic tool delivery platform and a tissue approximation device for percutaneous beating-heart closure of a patent foramen ovale (PFO). The approach has been validated with *in vivo* large animal experiments, which demonstrated a novel alternative to both catheter-delivered PFO closure devices and to surgical closure by suture (Gosline et al., 2012a; Vasilyev et al., 2013).

This paper considers the task of tissue removal inside the beating heart. Tissue removal is an essential component of both pediatric and adult intracardiac procedures and predominantly involves either removal of abnormal tissue or creation of communication between cardiac chambers or great vessels. Examples of abnormal intracardiac tissue are membranes above or below heart valves and abnormal muscle bundles in the heart ventricles (see Figure 1(b)), which create obstruction of the normal blood flow and subsequent heart dysfunction.

Current treatment consists of either plastic deformation of the obstructing tissue by balloon dilatation, in catheter-based techniques, or partial to complete tissue removal via

open-heart surgery. The major limitation for balloon dilatation, however, has been achieving a balance between dilating or tearing the abnormal tissue as opposed to the normal tissue that comprises the structure of the valve or sub-valve area of the heart.

As a specific pediatric example, the abnormal obstructing tissue in the right ventricle is usually elastic. This makes balloon dilatation ineffective, since inelastic deformation is nearly impossible to achieve without damage to normal valve structures. Therefore, the only currently available form of treatment is open surgical removal of the abnormal tissue, which requires use of cardiopulmonary bypass. The procedure can involve removing several cubic centimeters of tissue.

An important example of the creation of an artificial communication between cardiac chambers is atrial septostomy (Figure 1(c)), in which a hole or artificial interatrial communication is created between the left and right atria. It is usually indicated for patients with severe pulmonary hypertension as a procedure of last resort in order to prevent heart failure. The procedure currently is performed by catheter and involves transseptal puncture and repeated balloon dilatations of the atrial septum. Complications are quite high and related to the critical condition of these patients and often to cardiac perforations due to technical problems during transseptal puncture (Kurzyna et al., 2007).

The contributions of this paper are the design, fabrication and validation of a robotically controlled, steerable tissue removal device for surgery inside the beating heart. A concentric tube robot platform is used to deliver a novel metal MEMS tissue removal tool. Two demonstration procedures are presented. The first involves *ex vivo* tissue removal from the outflow tract of the right ventricle. The second addresses *in vivo* atrial septectomy in a porcine model. Added contributions in this paper beyond conference publication (Gosline et al., 2012b) include robot design in Section 4, robot control in Section 4.3, optimization of the cutting process in Section 5.1, and the addition of an *in vivo* validation experiment in Section 5.3.

For both demonstration procedures, the robot enters the heart percutaneously from the right internal jugular vein, as shown in Figure 1(a). In the first procedure, the robot passes through the tricuspid valve into the right ventricle. In the second procedure, the robot is navigated to the atrial septum. Once properly positioned with respect to the tissue, the tool can be employed to remove tissue. The robot lumen transports power to the tool through a flexible drive shaft while also providing integrated irrigation and aspiration so that the morselized debris can be transported out of the heart through the lumen of the robot. Irrigation using heparinized 0.9% sodium chloride solution facilitates transport while minimizing both blood loss and device clogging due to emboli formation.

The paper is arranged as follows. The next section describes the metal MEMS manufacturing technology used

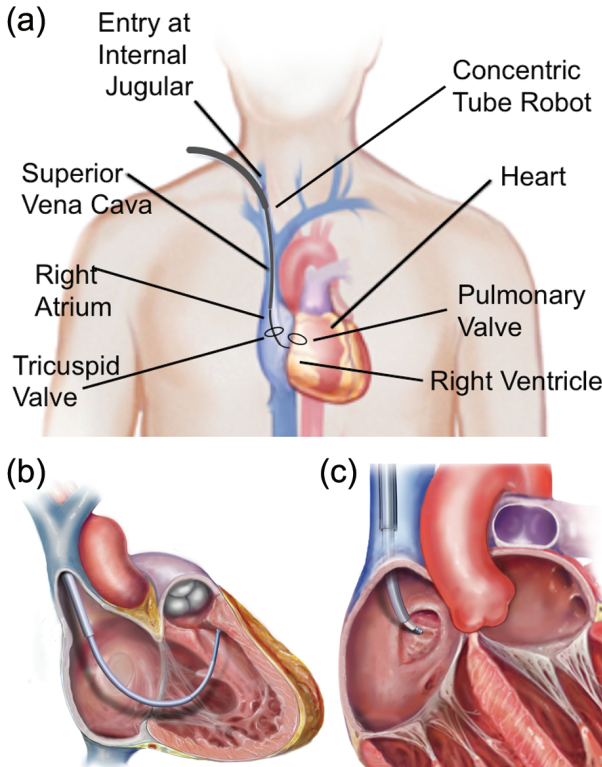


Fig. 1. Concentric tube robot entering the beating heart to perform two demonstration procedures. (a) Percutaneous entry via the internal jugular vein. (b) Tissue removal from the right ventricular outflow tract. (c) Tissue removal from the atrial septum – creation of an artificial communication between right and left atria.

to fabricate the device. The following section describes the surgical requirements and design of the device. Next, the design of a concentric tube robot for tool delivery is described and the integration of the cutting tool is detailed. A description of the *ex vivo* and *in vivo* experimental results is then provided. The findings are discussed in the final section.

2. Metal MEMS fabrication technology

Presently, millimeter-scale surgical devices are manufactured in metal using conventional methods such as computer numerically controlled (CNC) machining, electrical discharge machining (EDM), laser cutting, or grinding. Additionally, much micro-electromechanical systems (MEMS) research involves creating components out of silicon wafers using techniques that were adopted from solid-state electronics and microchip manufacturing. These available technologies have significant limitations, when it comes to making functional assemblies of moving parts at the millimeter scale that have to perform surgical functions such as approximate or remove tissue. Silicon is a brittle material, and conventionally machined metal parts are difficult to make, inaccurate, or are expensive to assemble.

Unlike prior art, the MEMS technology used here (Microfabrica Inc, Van Nuys, CA) is an additive, lithography-based manufacturing process that can create intricate three-dimensional (3D) shapes with moving parts without assembly (Cohen et al., 1999). The process involves depositing successive layers of a structural material (e.g. NiCo) and a sacrificial one (Cu), as illustrated in Figure 2. The presence of a sacrificial layer allows for creation of overhangs, bearing surfaces, and multi- part assemblies all in one manufacturing step. The parts are released in the final step of the process by etching away the sacrificial material.

Since the method relies on selectively electroplating the structural material, its layers feature excellent adhesion, with the final manufactured parts exhibiting structural properties similar to those of a monolithic material (Simaan et al., 2009). Thus, the process allows designers to transform complex assemblies with moving parts, hinges, bearings, and threads with feature sizes of a few microns directly from CAD renderings to metal parts. Finally, as a batch manufacturing technique, it allows large volume production of parts at low cost. This manufacturing process has been previously used by our group to create a tissue approximation device for PFO closure (Gosline et al., 2012a; Vasilyev et al., 2013).

3. Device design

Standard techniques for surgically removing tissue inside the heart include the use of forceps with scalpel blade or scissors to retract, cut and remove the desired tissue. Since the heart is stopped, tissue debris can be manually picked up and removed as well as flushed from the heart chambers without risk of debris escaping into the bloodstream where it could create emboli. Recreating the full range of tissue removal techniques that an experienced surgeon can accomplish with hand held tools is extremely challenging for a robotic system. An appropriate strategy for designing a robotic tissue removal tool, however, is to consider the requirements of the tissue removal tasks as well as the constraints imposed by the surgical environment and those of the robotic delivery system. In this way, the tool design requirements can be grouped as surgical requirements and robot delivery requirements.

Surgical requirements include:

- (1) Tissue to be removed may consist of only thin endocardial surface layers or may form thick muscular myocardial layers.
- (2) Tool must effectively cut (without excessive tearing) abnormal endocardial tissue, which is strong and elastic.
- (3) Tissue debris cannot escape into the blood stream if it is large enough to create emboli. Blood is composed of particles ranging from 2 to 120 μm in size. Clinical significance of emboli depends on the size of the individual emboli and the number of them flowing at the same time. Endovascular filters are typically used

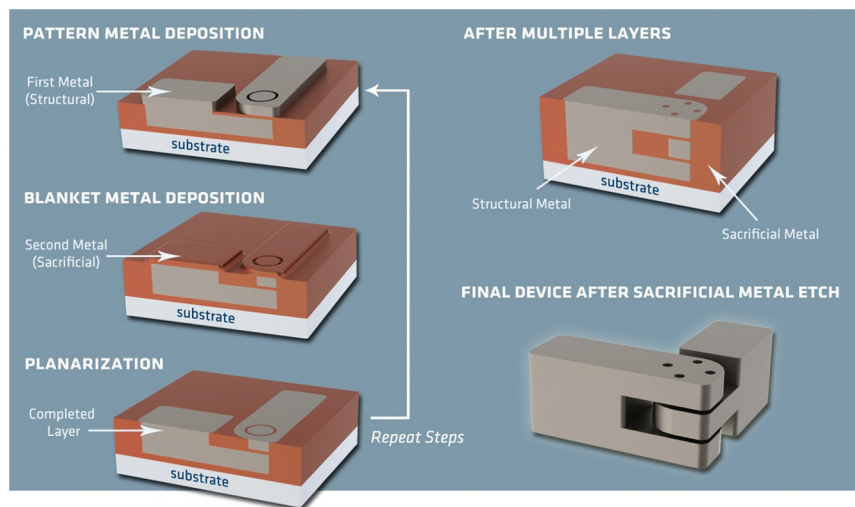


Fig. 2. Metal MEMS fabrication process – revolute joint example. The formation of each layer involves three steps: pattern deposition of a structural metal, blanket deposition of sacrificial metal, and planarization. After all layers are formed, the sacrificial metal is removed, leaving behind the assembled 3D device.

clinically for protection from emboli. The smallest pore diameter in currently available filter devices is about 40 μm , with the majority of filters having an 80 to 100 μm pore diameter (Kasirajan et al., 2003). For the purpose of this study, we set the debris size of 50 μm as a critical size. In the future studies, we are planning to capture and characterize the debris.

- (4) Blood loss arising from aspiration should be limited (allowable blood loss depends on an individual patient's weight and hematocrit; it is calculated as follows: allowable blood loss = [patient weight \times average blood volume for this age/sex group \times (initial hematocrit – lowest acceptable hematocrit)] / lowest acceptable hematocrit [Gross, 1983].

Robotic delivery requirements include:

- (1) Tool/robot diameter is limited to 3 mm to enable percutaneous delivery through the vasculature in children and adults (8 mm diameter catheters have been used for adult aortic valve replacement).
- (2) Cutting tool power must be delivered through the robot as its curvature and length varies.
- (3) Morselized tissue must also be evacuated through the lumen of the robot without becoming jammed in either tool or lumen.

Together these requirements can be combined to produce a set of tool design requirements as described below.

Functional design requirements:

- (1) Tool must be capable of cutting tissue at its tip in order to enable removal of thick muscular layers.
- (2) To provide precise control for the removal of surface layers, tool should have a cutting guard that prevents undesired deep cutting as a result of cardiac cycle motion.

(3) The tool design should be scalable in diameter in order to provide the means to trade off tissue removal precision with removal rate.

(4) To ensure entrainment and transport of tissue debris while minimizing blood loss, tool should provide integrated irrigation as well as aspiration.

No existing medical devices meet these functional requirements. While there are biopsy catheters, they are only capable of taking small bites of tissue and so cannot be used effectively for either the removal of area surface layers or the removal of a significant amount of tissue. Existing powered instruments for the mechanical removal of tissue are typically too large and are designed as a pair of concentric closed rotating tubes with a cutting window on the side. Tissue removal depends on the herniation of tissue into the window - a design that has limited effectiveness at small diameters and for smooth tissue surfaces. Furthermore, since the cutting window is located on the side of the tip of the tool, they are incapable of performing plunge cuts or sculpting the tissue to create a desired surface profile. Thus, a completely new tissue removal technology is needed to meet the functional requirements.

3.1. Design features

Unlike the machining of stiff materials such as bone and metal, a cutting device for soft tissue cannot rely on the reaction force of the tissue to generate sufficient force for cutting. Furthermore, capture of debris necessitates a cutting action in which the tissue 'chips' that are generated are entrained in a flow leading into the cutter head and not the bloodstream. These requirements suggest a stator/rotor tool geometry for producing a scissoring action on the tissue.

We have manufactured several cutter designs, one of which is depicted in Figure 3. The light gray component

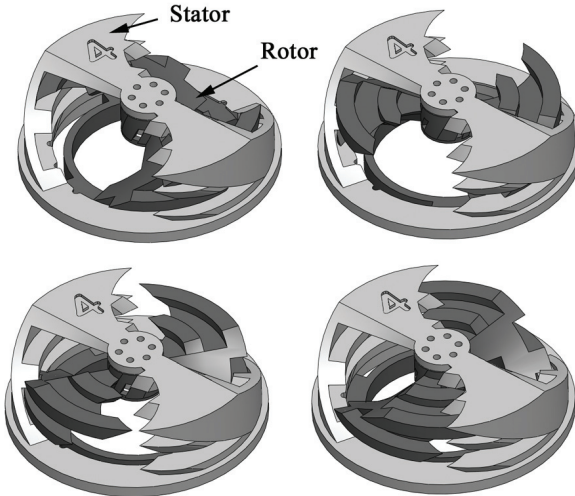


Fig. 3. Tissue removal tool design depicted at four angles of rotation.

acts as the stator and is fixed to the distal tube of the robot. It includes two large cutting windows 180° apart. The rotor, shown in dark gray, rotates relative to the stator and possesses two sets of five sharp cutting teeth that grab any tissue projecting into the cutting windows of the stator.

The sharp leading edges of the stator and the rotor enable the device to grab and slice the tough endocardial tissue layer. The multiple sets of interlocking teeth in each window ensure that the entrained tissue is cut into smaller pieces. Ideally, morsel size should be about one-tenth the diameter of aspiration lumen to aid transport and minimize the potential of clogging. The number of teeth is selected to balance this desired bite size with mechanical strength of the cutting components.

Even though the tool will not be operating while it is being navigated over the surface of the beating heart to the surgical site, it is important to provide the means for avoiding accidental tissue damage that could occur if the sharp edges of the tool dig into the tissue. To prevent this, the outer portions of the stator between the cutting windows function as cutting guard surfaces. When the tool is drawn under light pressure across tissue such that the stator guards are in contact, the tissue is protected from these sharp edges – even when the tool is operating. To perform cutting, the tool must be activated and displaced with respect to the tissue such that the tissue is directed into the cutting windows. Note, however, that if the tool tip is pressed into the tissue surface, cutting can occur regardless of orientation. While not discussed here, we are currently developing the capability to retract the cutting head into the robot tip to protect against accidental penetration and cutting.

Since the MEMS fabrication process used to create these tools builds the devices from thin planar layers, device cost and complexity is closely tied to the number of layers. An advantage of the rotor-stator design is that its diameter can

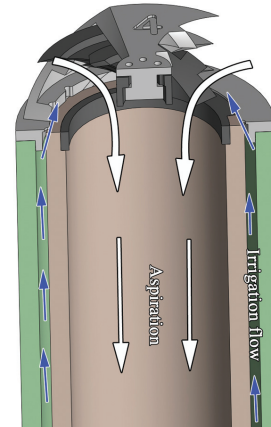


Fig. 4. Cutaway view of the tissue removal tool to illustrate fluid flow. The outer annular channel supplies heparinized saline while the inner channel provides aspiration to remove debris.

be easily scaled, e.g. from 1–5 mm, using approximately the same number of layers. The depicted version has a diameter of 2.1mm and was fabricated using 36 layers, each 25 μm thick. The number of mating cutting teeth can be scaled with diameter to control bite size, although larger diameter aspiration lumens are also capable of accommodating larger debris.

As shown in Figure 4, the rotor is attached to and driven by a flexible rotating tubular drive element with a suction source connected to its lumen at the proximal end. The rotor is attached to the stator through a journal bearing as shown in the cut-away. While the bearing can support both axial and radial loads, the drive system has been designed to minimize axial bearing loads, as described in Section 4.2. A small gap between the drive tube and the innermost (distal) robot tube is used to pump heparinized saline into the chamber between the rotor and stator. While the rotor can be run dry when not cutting, this irrigating flow serves as a lubricant. During cutting, it serves to transport debris through the aspiration lumen with minimal blood loss, while use of heparin prevents the formation of emboli inside the device and aspiration lumen.

4. Robot design and tool integration

Concentric tube robots, shown in Figure 5, are comprised of pre-curved elastic tubes in a telescopic arrangement. Each tube can be translated and rotated relative to the other tubes to generate shape change. Our group has previously developed design guidelines for concentric tube robots in which each section along the length of the robot can have either a fixed or a variable curvature (Dupont et al., 2010). A fixed curvature section is comprised of a single tube and possesses two degrees of freedom (DOF) corresponding to extension and rotation. A variable curvature section is comprised of two tubes that extend together. It possesses three DOF corresponding to extension, rotation, and varying curvature. Each section is also designed to be (approximately)

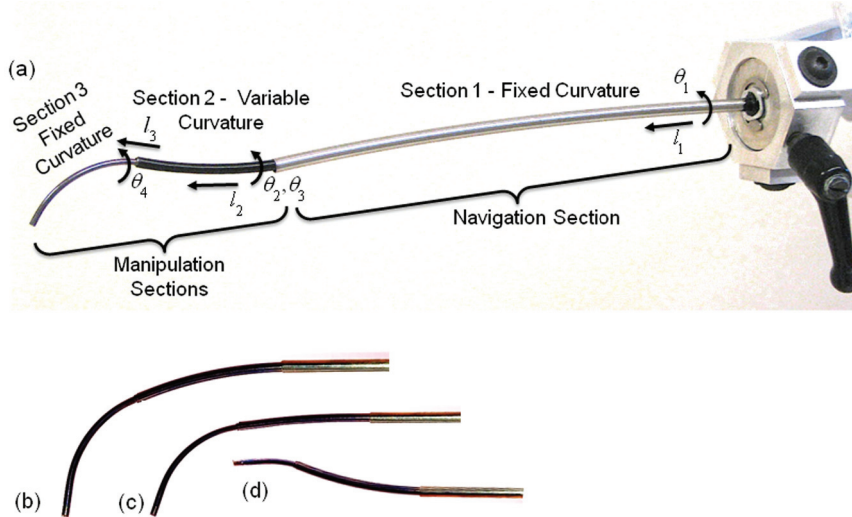


Fig. 5. Concentric tube robot for tissue removal. (a) Robot sections and degrees of freedom. (b) Section 2 at maximum curvature. (c) Section 2 at minimum curvature. (d) Section 3 partially retracted inside section 2.

kinematically decoupled from its proximal sections. This is achieved by selecting the bending stiffness of each section to dominate that of its distal sections.

Using this approach, a robot design for beating-heart closure of PFO was previously described in (Gosline et al., 2012a; Vasilyev et al., 2013). Since the tissue removal experiments described in this paper require targeting similar locations inside the heart, the design used here is also comprised of three sections and possesses seven DOF, as shown in Figure 5.

The proximal section is of fixed curvature and is used to navigate from percutaneous entry of the internal jugular vein into the right atrium (Figure 1(a)). Once positioned, this section can often be locked for the duration of the procedure. In contrast, the two distal sections, possessing variable and fixed curvature, respectively, actively position and orient the robot tip during the procedure. These two sections possess five DOF with the missing DOF corresponding to tool roll.

While the number, type and curvatures of the robot sections used here correspond to the design of (Gosline et al., 2012a; Vasilyev et al., 2013), the individual tube diameters are different since they must be selected to match the size of the tool or device being delivered. The tissue removal tool selected for testing has an outer diameter of 2.1 mm. As described in the following subsection, the tool is mounted to the tube comprising the distal robot section. As shown in Figure 4, the tube outer diameter is selected to match that of the tool. The inner diameter is selected to fit against the tool collar as also shown in Figure 4 and to accommodate a flexible drive tube with an outer diameter of 1.5 mm.

These diameters fully define the fixed-curvature section 3, as given in Table 1. The diameters of the two tubes

comprising variable-curvature section 2 are selected subject to several constraints. These include achieving equal bending stiffnesses for the two tubes while also producing a composite bending stiffness that dominates that of section 3. Additional constraints considered include bending strain at maximum curvature, tube ovalization and buckling. While the details of the calculations are beyond the scope of this paper, the tube diameters given in Table 1 produce the desired curvatures and provide a stiffness ratio of 0.9950 with respect to each other and a combined stiffness ratio of 6.1 with respect to section 3. A ratio of this size has proven adequate to obtain approximate decoupling of motion between sections 2 and 3. For improved visualization in ultrasound, section 2 was covered with ~ 0.25 mm thick thermoplastic heat-shrink tubing. Finally, given a coated outer diameter of section 2 of about 3.5 mm, section 3 was similarly designed. Fabricated from stainless steel, the stiffness ratio of it with respect to the three tubes of sections 2 and 3 is 8.8.

Owing to their construction, concentric tube robots are stiffer than standard catheters. While little data is available on the stiffness of robotic catheters, our prior work using a design comparable to the one described here has shown that deflections of 1–2 mm can generate forces exceeding the maximum of 27 g that can be produced by the Magnetecs magnetic catheters (Vasilyev et al. 2013). This is to be expected since concentric tube robotic catheters are intended for procedures involving the control of large tip forces, such as tissue manipulation. In contrast, magnetic catheters are designed to produce the small contact forces appropriate for ablation.

For tissue removal, catheter stiffness is needed to minimize the vibrations induced by high-speed rotation of the

Table 1. Concentric tube robot design parameters. Section numbers are from right to left in Figure 5(a).

	Navigation	Manipulation	
Section	1	2	3
Curvature type	Fixed	Variable	Fixed
Material	Stainless steel	NiTi	NiTi
Maximum section length (mm)	200	45	35
Radius of curvature (mm)	800	80–∞	25
		Outer tube	Inner tube
Inner diameter (mm)	4.27	2.750	2.215
Outer diameter (mm)	4.78	3.000	2.631

cutting tool and to control tip position during cutting. High stiffness inside the beating heart, however, increases the potential for over-penetration and perforation. For this reason, the initial *in vivo* results described in this paper target a procedure, atrial septostomy, in which perforation is the goal. Ongoing research is addressing control of cutting depth for other procedures.

4.1. Tool-robot mounting

It is generally preferable to design tools for insertion and removal through the proximal end of the robot lumen. This approach enables the robot to remain in position inside the body while a tool is changed. This approach was utilized for the tissue approximation device reported in (Gosline et al., 2012a). For high-speed rotating tools, however, this method presents challenges since tool rotation and cutting require the application of torques between two tubular elements. By utilizing the distal robot section as the outer tubular element of the transmission, the torsional stiffness is maximized for a given outer diameter.

Consequently, the tissue removal tool with attached flexible rotating drive tube was mounted to the robot by insertion from the distal end. Thus, the tool cannot be changed while the robot is inside a patient. The tool assembly was connected to the tube comprising the distal section by means of mating snap connectors, as shown in Figure 6. The four snap connectors are positioned axisymmetrically and were created by laser cutting the NiTi robot tube. This design allows for axial and radial alignment as well as torque transmission, while ensuring easy and accurate assembly/disassembly.

Since the manipulation sections of the robot lack the DOF corresponding to tool roll, it is important to accurately position the two cutting windows of the tool with respect to the curvature of the third robot section. Thus, the snap connectors are located circumferentially such that two of the dog-bone cutouts on the tool assembly are centered in the cutting windows (see Figure 6(b)). The four matching male dog-bone protrusions on the robot tube were arranged so that the cutting windows could either be positioned in the plane of curvature of the third robot section (Figure 6(c))

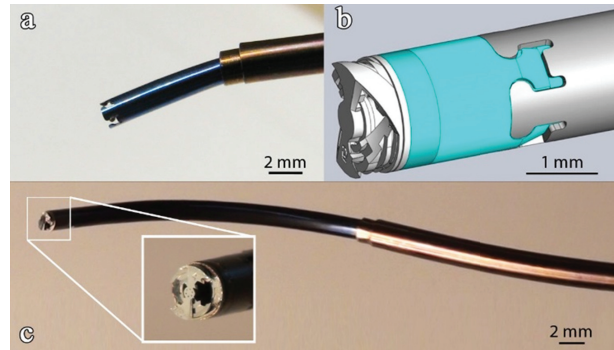


Fig. 6. Snap-in mounting system to connect tissue removal tool to the distal NiTi robot tube. (a) Robot showing laser cut dog-bone pattern. (b) CAD model showing assembled tool and robot. (c) Actual assembly.

or, by rotating the tool assembly 90°, could be oriented orthogonal to the curvature plane. The preferred cutting orientation is discussed in the subsection on robot control below.

4.2. Tool drive system

The tool drive system was designed to attach to the proximal end of the robot drive stage controlling the distal robot section, as shown in Figure 7. Since this section is constant curvature, it is comprised of a single tube driven by a two DOF stage (one rotation and one translation). This stage was designed to include a mounting flange to mate with the tool drive system. The flexible tool drive tube passes through the entire length of the robot and mates with the tool drive.

As shown in Figure 4, design of the speed-controlled tool drive is complicated by the need to deliver torque through a rotating tubular component that also acts as the boundary between two fluid flows. This challenge is addressed through a system of seals that separate the irrigation flow on the outside of the drive tube from the aspiration flow through its lumen.

A second design challenge arises from the curvature of the robot, which varies during operation, combined with the

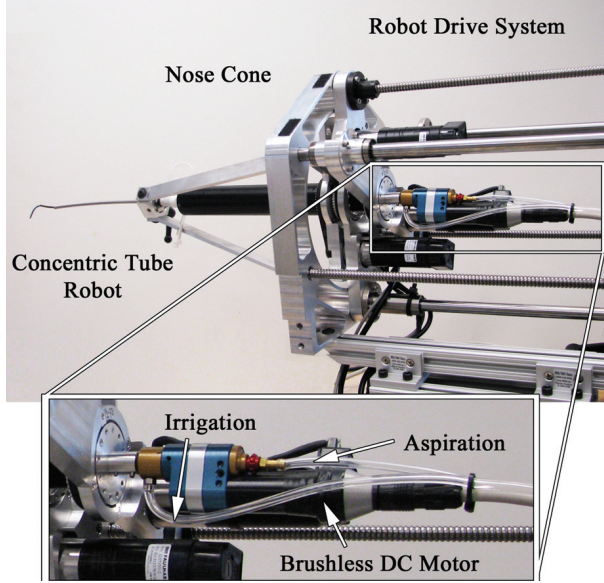


Fig. 7. Concentric tube robot showing tool drive mounted on distal section drive stage. Inset provides detail view.

finite clearance between tubes. These factors create slight variations in the arc length of the rotating transmission tube that can generate damaging axial loads. To accommodate this axial play, a floating gearing system was designed to allow 3 mm of axial motion without gear binding.

A brushless DC motor (Faulhaber, DE) with integrated Hall effect sensors was chosen for the drive system because of its high torque, compact diameter, and speed control electronics. The motor is driven with a three phase, PWM motor driver (Faulhaber, DE) at 24 V DC and provides a tool speed range of 0–5000 rpm. The components of the tool drive are shown in Figure 7.

To provide irrigation of the cutting tool with heparinized saline, a variable speed peristaltic pump (OmegaFlex FPU422, Omega Engineering, Inc.) with a flow rate of 32–200 mL/min was used, as shown in Figure 8. The benefit of this type of pump is that the fluid is sealed from contamination as it travels through disposable, pre-sterilized tubing. For aspiration of cutting debris, a portable suction unit (Schuco Vac 330, Allied Healthcare Products) was used. This device employs a reciprocating pump, and supplies negative pressure from 1–18 inHg with fluid and debris collected in a 700 cc canister.

4.3. Robot control

The robot controller provides two modes of operation, as shown in Figure 9. The first involves teleoperated control of robot tip position and orientation while the second utilizes keyboard control of individual and group motions of the tubes. Cutting experiments were performed, as described in section V below to compare control input modes as well

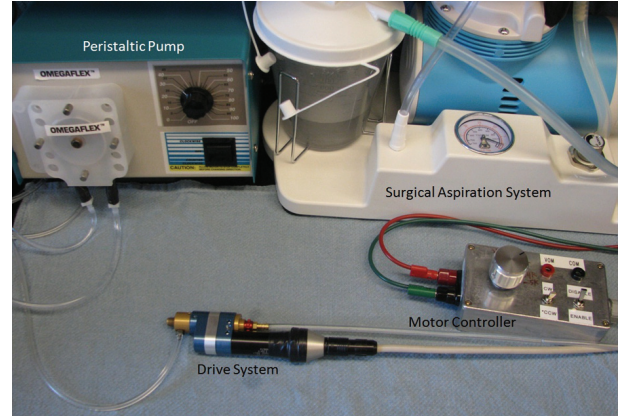


Fig. 8. Components of the tool drive system.

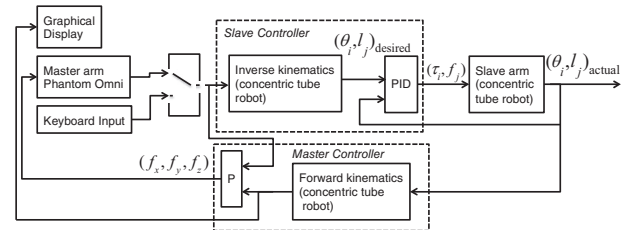


Fig. 9. Control system block diagram.

as to determine the best orientation of the cutting tool windows with respect to the curvature plane of the third section (Figure 6(c)).

5. Experiments

Three sets of experiments were performed to evaluate the tissue removal tool and its robotic delivery system. The first set of experiments was designed to evaluate the best tool motions and orientations for tissue removal and also to compare the teleoperation control modes of joystick versus keyboard input. The second set of experiments evaluated the potential for percutaneous removal of right ventricular outflow tract obstructions (removal of a thin endocardial layer followed by removal of a substantial amount of myocardium). These experiments were performed on *ex vivo* porcine hearts. The final experiment demonstrated percutaneous beating-heart tissue removal through an *in vivo* atrial septostomy (removal of thin dense tissue, while creating a patent circular or oval communication between the atria). These experiments are described below.

5.1. Optimization of the cutting process

In the first set of experiments, a handheld tool was used to investigate the orientation of the tool axis with respect to the tissue surface normal and with respect to the relative motion between the tool and tissue. These experiments revealed that the best cutting performance was obtained when the axis of the cutting tool was oriented at 45° with respect to the tissue surface normal and the tool was rotated about its

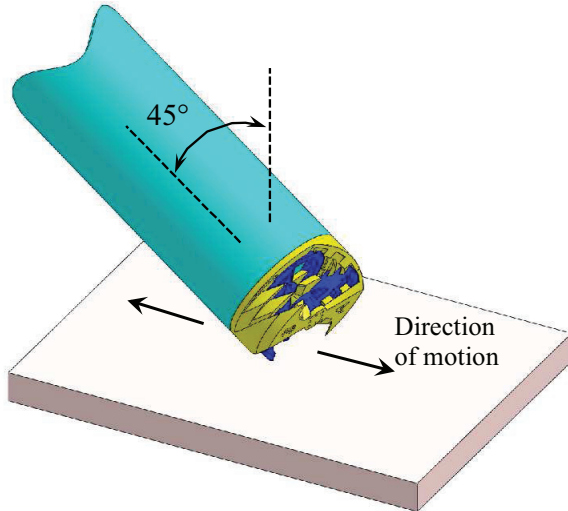


Fig. 10. Desired orientation and motion of tool for effective cutting.

axis so as to align the tissue surface with the cutting window (Figure 10). This roll angle orientation exposes the most tissue to the cutting surfaces. It was also observed that at this orientation, pulling the cutting tool across the tissue surface produced a stable sliding motion while pushing it across could occasionally cause the tool to pivot and push into the surface.

5.1.1. Selection of cutting parameters. Experimentally determined values of the motor rotation rate, irrigation flow, and aspiration pressure were obtained by *ex vivo* testing of cardiac tissue. Variation of the rotation rate has a considerable effect on the cutting behavior. Increasing tool rotation rate results in a reduced tissue ‘bite’ size for a given feed rate. This can have two beneficial effects. Smaller bite sizes, particularly of elastic tissue, such as endocardium, are less likely to jam the tool. Secondly, smaller pieces of debris can be more readily transported into and through the robot lumen. For less fibrous tissue such as myocardium, however, a high cutting speed can result in clouds of very small particles, which can be harder to fully entrain in the flow. Given these factors, a high rotational speed was found best for removing the endocardial layer (~ 1500 rpm) and a slower speed (~ 1000 rpm) for myocardial tissue.

The amount of tissue debris left behind during cutting depends not only on rotational rate, but also on depth of cut and feed rate as well as irrigation rate and aspiration pressure. If the depth of cut exceeds the height of the cutting window (~ 1 mm), the tissue is torn as the tool is moved across its surface. Similarly, tissue tearing occurs if feed rate exceeds the capacity of the tool to cut and remove debris.

Precise control of cutting depth and feed rate is currently only possible during *ex vivo* experiments owing to heart motion and imaging limitations during beating-heart procedures. During handheld testing, the aspiration and irrigation

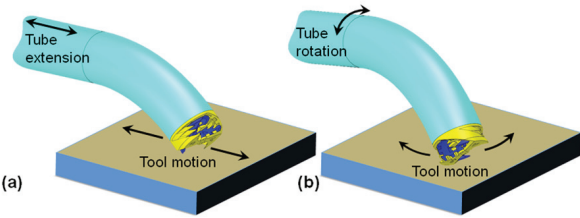


Fig. 11. Robot section motions and the associated tool motions. (a) Section extension with depicted fixed tool roll angle produce tissue removal conditions of Figure 10. (b) Tool roll angle is rotated 90° and section rotation is used to prevent over-penetration during tissue removal.

parameters were iteratively adjusted to achieve no net fluid loss while capturing all visible debris during precisely controlled *ex vivo* cutting. At settings of 15 inHg vacuum and 100–150 mL/min flow, there is an accumulation of fluid on the cutting surface, but no visually observable tissue debris.

5.1.2. Teleoperative control during cutting. In *ex vivo* tests, it was observed that the desired cutting motion of Figure 10 could be produced using teleoperation. Based on previous robotic *in vivo* experiments, however, the noise and limited resolution of 3D ultrasound imaging make it difficult to perform accurate relative motions between the robot tip and intracardiac tissue. Consequently, an alternate approach was adopted in which small-amplitude oscillatory motions of tube degrees of freedom could be used to produce computer-controlled tool-tissue motion. These motions can be produced either through teleoperative control or through keyboard commands. The two candidate motions correspond to oscillatory robot extension and rotation of the distal robot section, as shown in Figure 11.

Notice that the roll orientation of the cutting tool differs for the two cutting motions. For robot extension, the cutting windows must be placed in the plane of curvature (Figure 11(a)) to expose the tissue. This configuration produces tool-tissue motion matching Figure 10. For robot section rotation, the tool is rotated 90 degrees so that the cutting windows are directed orthogonal to the plane of curvature (Figure 11(b)) such that tool motion forces tissue into the cutting windows.

Of these two section-based robot motions, distal section rotation is safer since at the position of maximum displacement into the tissue, the tissue presses against a cutting guard rather than against a cutting window. In contrast, oscillatory robot extension has the potential to produce its most aggressive cutting at maximum extension.

Thus, the final tool assembly was mounted to the robot in the configuration of Figure 11(b). For tissue removal, the robot tool tip could be pressed against the tissue at a desired location. The tool could then be activated and the distal section oscillated $\pm 20^\circ$ from its initial value for several cycles to remove the underlying tissue. Next, the tool could be

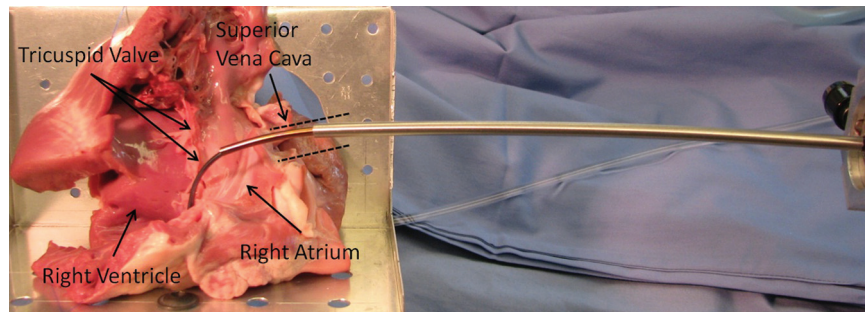


Fig. 12. Experimental set up for removal of right ventricular outflow tract obstructions.

turned off and the robot tip repositioned with respect to the initial location. Tool activation and section oscillation could then be repeated so as to obtain the desired pattern of tissue removal.

This procedure made it possible for the cardiovascular surgeon to use both hands to operate the ultrasound imaging system while providing robot motion commands orally to an assistant. As described above, these commands consisted of positioning commands, specifying for example, a relative displacement of several millimeters described in tip coordinates. This would be followed by a request to initiate irrigation, aspiration and cutter motor power and then a request to roll the distal section $\pm 20^\circ$ in increments of 5° for several cutting cycles. The assistant input the commands to the controller using the keyboard and graphical display interface.

5.2. *Ex vivo* removal of right ventricular outflow tract obstructions

Ex vivo experiments using porcine hearts were performed to develop a percutaneous procedure for the removal of obstructions from the right ventricular outflow tract. The proposed procedure (Figure 1(b)) involves entering the heart from the internal jugular and navigating into the right atrium via the superior vena cava. The robot navigates through the tricuspid valve by passing through a commissure to ensure that the valve can continue to operate during the procedure. Reaching the right ventricular outflow tract, the proximal navigation sections of the robot are then held fixed while the distal manipulation sections are teleoperated to sweep the tissue removal tool over the excess tissue and so remove it.

The experiment is shown in Figure 12. A porcine heart from a local slaughterhouse was immobilized by suturing it to an aluminum fixture. The heart was then cut open from the entry point at the superior vena cava, through the right atrium, the tricuspid valve, and into the right ventricle to enable the documentation of the robot path and the progression of cutting. Finally, the heart and fixture were placed in an anatomically correct location with respect to the robot for entry at the internal jugular vein.

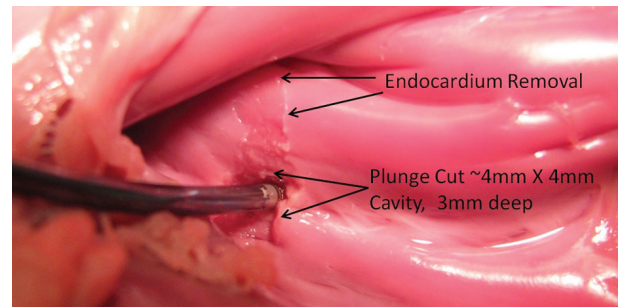


Fig. 13. *Ex vivo* robotic tissue removal near the outflow tract of the pulmonary valve. Illustrated cutting tasks include removal of endocardial surface layer and bulk removal of myocardium.

Figure 13 illustrates typical results from the cutting experiments on two types of tissue. Near the top, removal of the endocardial surface layer was performed with a gentle sweeping motion along the surface, with the tool positioned at an angle of 45° from normal. Note that the underlying muscular tissue is exposed, and that the shiny, smooth endocardium has been removed in a roughly rectangular pattern. Lower down in the figure, a cavity was milled into the tissue by pressing the tool into the tissue with a normal approach and sweeping it in a small circular pattern to expose the surrounding tissue to the cutting windows of the tool.

5.3. *In vivo* atrial septostomy

To demonstrate *in vivo* tissue removal inside the beating heart, a surgery was performed on a 70.4 kg Yorkshire swine. This species was selected owing to the similarity between its heart and the human heart. Atrial septostomy was selected as an initial clinical target procedure because it does not involve the risk of accidental perforation during the procedure, but rather involves deliberate penetration of the atrial septum and enlargement of the hole created. (The experimental protocol was approved by the Boston Children's Hospital Institutional Animal Care and Use Committee. The animal received humane care in accordance with the 1996 Guide for the Care and Use of Laboratory Animals recommended by the US National Institutes of Health.)

The procedure was performed by a single operator who was a trained cardiovascular surgeon with prior experience

in the development of image-guided cardiac procedures (NVV), and an assistant (AHG). The operator controlled the X-ray angiography station and the ultrasound system. The assistant, positioned on the opposite side of the table, operated the robotic and tool controls taking commands from the operator.

The animal was anesthetized by intramuscular injection of tiletamine/zolazepam (7 mg/kg) and xylazine (4 mg/kg), intubated with a cuffed endotracheal tube and ventilated with a volume control ventilator (Hallowell EMC Model 2000; Hallowell EMC, Pittsfield, MA). Anesthesia was maintained with 2% to 3% isoflurane.

A midline sternotomy was performed, and an initial assessment of the intracardiac anatomy was completed using epicardial echocardiography using the X7-2 matrix transducer on an IE33 system (Philips Healthcare, Andover, MA). After heparin was administered at 150 U/kg intravenously, a right side neck cut-down approach was performed and the right internal jugular vein was identified.

The robot lumen is initially flushed with heparinized saline and inserted under 3D ultrasound guidance through a previously introduced 16-French introducer sheath (Cook Medical Inc, Bloomington, IN), which extends through the vasculature and just into the right atrium. All robot insertion and retraction motion is with respect to the sheath and not the vasculature.

As the navigation section of the robot (Figure 5) entered the right atrium, 3D echocardiography was supplemented with X-ray fluoroscopy (XRE corporation angiography station, Littleton, MA) to confirm its location. The navigation section was manually navigated to the middle portion of the right atrium and then locked in place for the duration of the procedure.

The manipulation sections of the robot (Figure 5) were then extended from the navigation section under keyboard command and guided to the atrial septum, as shown in Figure 14. While these ultrasound images are noisy, heart motion as visualized by the 30–35 Hz update rate aided distinguishing the robot from the surrounding tissue. Furthermore, the ability of the robot to remain in a fixed configuration during echocardiography greatly facilitated the procedure.

Tool contact with the septum was confirmed visually by immobilization of the septal tissue over the cardiac cycle. The robot was then slightly retracted to reduce the contact force and the distal section was then rotated 20° clockwise to bring it out of contact with the tissue. Irrigation and aspiration were then initiated and the tool was powered on. The distal section was then rotated ±20° from the orientation of initial contact to produce a sweeping motion across the septum. By repeating this oscillatory motion while also varying the robot extension length and penetration depth into the tissue, penetration through the full thickness of the septum was achieved. This was confirmed by 2D and 3D echocardiography as well as color Doppler imaging. As shown in Figure 15, ultrasound measurements revealed a 4.5 mm

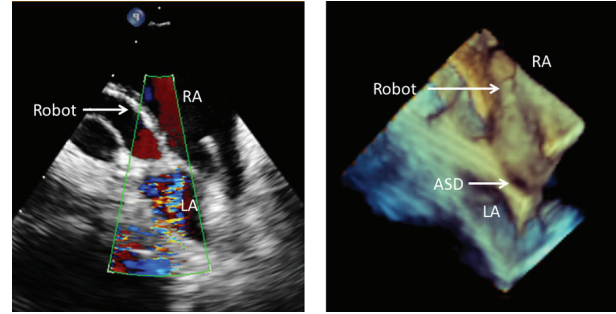


Fig. 14. Robot navigated toward atrial septum under 2D echocardiography with color Doppler imaging (left) and real-time 3D echocardiography (right). RA – right atrium, LA – left atrium.

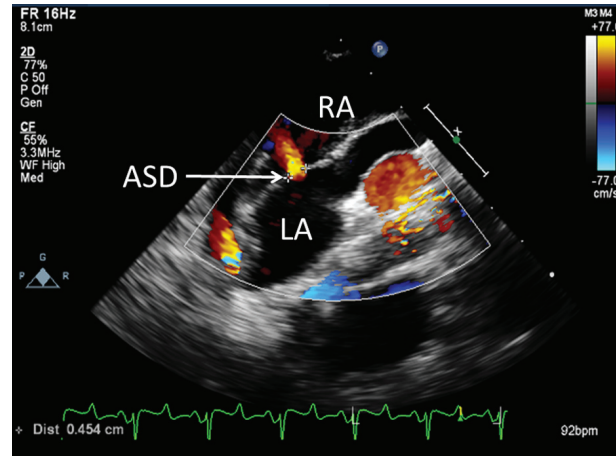


Fig. 15. 2D color Doppler imaging shows the 4.5 mm ASD that was created. RA – right atrium, LA – left atrium.

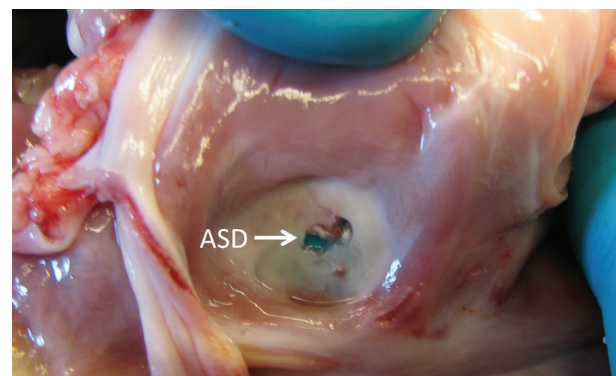


Fig. 16. Post mortem view of created atrial septal defect (ASD). View from the right atrium.

wide opening allowing blood flow from the left to the right atrium. The robotically created atrial septal defect was also confirmed by direct inspection, as shown in Figure 16.

6. Conclusions

Successful application of robotics in surgery necessitates the creation of new approaches, techniques and tools. This

paper provides such an approach to a previously unaddressed clinical need - removing tissue inside a beating heart. We have proposed and fabricated a solution that incorporates two promising novel technologies: metal MEMS tools and concentric tube robots.

The tissue removal tool demonstrated here possesses several important advantages. In contrast to existing microdebriders, it is able to remove tissue at its tip and, furthermore, its large cutting window enables tissue capture despite its small size.

The robotic tool delivery system provides a steerable yet stiff platform for controlling tool-tissue contact so as to enable precise tissue removal while also satisfying the stringent constraints of operating inside the beating heart. The approach was validated in porcine animal model and we successfully demonstrated both tool tip stability and cutting accuracy on a moving atrial septum.

Transition of beating-heart tissue removal to the clinic will involve addressing several challenges. First, while our experiments suggested that the majority of tissue debris was evacuated through the robot, further optimization of irrigation and aspiration parameters are needed to validate this observation. In addition, the use of catheter-deployed downstream embolization filters may be necessary to eliminate any risk of debris escape.

A second challenge to precise tissue removal is the imaging quality afforded by current echocardiography. While our team was able to successfully demonstrate atrial septostomy inside the beating heart, operating around delicate structures inside the heart could involve a significant learning curve and may pose higher patient risks. To address these challenges, our group is investigating alternate imaging modalities as well as contact force sensing.

Funding

This work was supported by the US National Institutes of Health (grant numbers R01HL073647 and R01HL087797).

References

- Cohen A, Zhang G, Tseng F-G, et al. (1999) Efab: rapid, low-cost desktop micromachining of high aspect ratio true 3-D MEMS. In: *IEEE international conference on micro electro mechanical systems*, Orlando, FL, USA, 21 January 1999.
- Camarillo D, Carlson C and Salisbury J (2009) Configuration tracking for continuum manipulators with coupled tendon drive. *IEEE Transactions on Robotics* 25(4): 798–808.
- Camarillo D, Milne C, Carlson C, et al. (2008) Mechanics modeling of tendon-driven continuum manipulators. *IEEE Transactions on Robotics* 24(6): 1262–1273.
- Dupont P, Lock J, Butler E, et al. (2010) Design and control of concentric tube robots. *IEEE Transactions on Robotics* 26(2): 209–225.
- Gander JW, Fisher JC, Reichstein AR, et al. (2010) Limb ischemia after common femoral artery cannulation for venoarterial extracorporeal membrane oxygenation: an unresolved problem. *Journal of Pediatric Surgery* 45(11): 2136–2140.
- Gosline AH, Vasilyev NV, Butler EJ, et al. (2012a) Percutaneous intracardiac beating-heart surgery using metal MEMS tissue approximation tools. *International Journal of Robotics Research* 31: 1081–1093.
- Gosline A, Vasilyev N, Veeramani A, et al. (2012b) Metal MEMS tools for beating-heart tissue removal. In: *Proceedings of the IEEE international conference on robotics and automation*, 2012, St Paul, MN, USA, 14–18 May 2012, pp. 1921–1936.
- Gross JB (1983) Estimating allowable blood loss: corrected for dilution. *Anesthesiology* 58(3): 277–280.
- Huang J, Triedman JK, Vasilyev NV, et al. (2007) Imaging artifacts of medical instruments in ultrasound-guided interventions. *Journal of Ultrasound Medicine* 26(10): 1303–1322.
- Ikeuchi M and Ikuta K (2009) Development of pressure-driven micro active catheter using membrane micro emboss following excimer laser ablation (MeME-X) process. In: *IEEE international conference on robotics and automation*, Kobe, Japan, 12–17 May 2009, pp. 4469–4472.
- Jayender J, Patel RV and Nikumb S (2009) Robot-assisted active catheter insertion: algorithms and experiments. *International Journal of Robotics Research* 28(9): 1101–1117.
- Kasirajan K, Schneider PA and Kent KC (2003) Filter devices for cerebral protection during carotid angioplasty and stenting. *Journal of Endovascular Therapy* 10(6): 1039–1045.
- Kesner S and Howe RD (2011) Position control of motion compensation cardiac catheters. *IEEE Transactions on Robotics* 27(6): 1045–1055.
- Kurzyna M, Dabrowski M, Bielecki D, et al. (2007) A trial septostomy in treatment of end-stage right heart failure in patients with pulmonary hypertension. *Chest* 131(4): 977–983.
- Madhani A, Niemeyer G and Salisbury J. (1998) The black falcon: a teleoperated surgical instrument for minimally invasive surgery. In: *IEEE/RSJ international conference on intelligent robots and systems*, Victoria, BC, Canada, 13–17 October, 1998, pp. 936–944.
- Menache CC, du Plessis AJ, Wessel DL, et al. (2002) Current incidence of acute neurologic complications after open-heart operations in children. *The Annals of Thoracic Surgery* 73(6): 1752–1758.
- Modi P, Rodriguez E and Chitwood WR Jr (2009) Robot-assisted cardiac surgery. *Interactive Cardiovascular and Thoracic Surgery* 9(3): 500–505.
- Rucker DC, Webster R III, Chirkjian G, et al. (2010) Equilibrium conformations of concentric-tube continuum robots. *International Journal of Robotics Research* 29: 1263–1280.
- Simaan N, Xu K, Kapoor A, et al. (2009) A system for minimally invasive surgery in the throat and upper airways. *International Journal of Robotics Research* 28(9): 1134–1153.
- Vasilyev NV, Dupont PE and del Nido PJ (2012) Robotics and imaging in congenital heart surgery. *Future Cardiology* 8(2): 285–296.
- Vasilyev NV, Gosline AH, Butler E, et al. (2013) Percutaneous steerable robotic tool delivery platform and metal MEMS device for tissue manipulation and approximation: initial experience with closure of patent foramen ovale. *Circulation: Cardiovascular Interventions* 6: 468–475.